Available online at www.sciencedirect.com
SCIENCE DIRECT®
International Journal of Multiphase Flow 31 (2005) 1015–1035
International Journal of Multiphase Flow
www.elsevier.com/locate/ijmulflow

Application of a level set method for simulation of droplet collisions

Sébastien Tanguy, Alain Berlemont *

UMR6614-CORIA, Technopôle du Madrillet, BP 12 Avenue de l'Université, 76801 Saint-Etienne-du-Rouvray Cedex, France

Received 8 December 2004; received in revised form 29 May 2005

Abstract

A level set technique for interface tracking is presented, both for the continuum surface force formulation and the ghost fluid method approach. A projection method is used to solve incompressible Navier–Stokes equations that are coupled to a transport equation for the level set function, defined as the algebraic distance to interface. Results are presented for head-on droplet collisions in coalescence and reflexive regimes with a 2D axi-symmetric code, and for an off-center droplet collision in a separation regime for a large impact parameter with 3D code. Simulations provided realistic and various droplet collision behaviors and they correspond to experimental observations.
© 2005 Elsevier Ltd. All rights reserved.

Keywords: Level set; Ghost fluid; Interface tracking; Droplet collision simulation

1. Introduction

Many industrial processes involve two or more interacting phases. Among them sprays are a wide field of research both for experimental studies and for modeling and numerical simulations. Although it appears more and more difficult to separate modeling and measurement problems, we are here only concerned with numerical simulations. In recent years numerous studies have been

* Corresponding author. Tel.: +33 2 32 95 36 17; fax: +33 2 32 91 04 85.
E-mail address: alain.berlemont@coria.fr (A. Berlemont).

0301-9322/$ - see front matter © 2005 Elsevier Ltd. All rights reserved.
doi:10.1016/j.ijmultiphaseflow.2005.05.010

devoted to two-phase flow modeling and, in particular, the transport processes of droplets in turbulent flows have been more and more precisely described by numerical simulations. However, it clearly appears that specific approaches must be developed when it is necessary to describe interface behavior. Numerical simulation studies on droplet collision thus remain a research topic of high interest for the modeling of droplet size distributions in sprays, both during the atomization process and droplet transport.

Such numerical studies have been carried out using either "front tracking" methods or "front capturing" methods. Front tracking methods (Nobari et al., 1996) are based on the Lagrangian tracking of marker particles that are attached to the interface motion. They appear suitable when irregularities on the interface curvature are not too large, but they are not well adapted to describing topological changes of the interface. In particular, droplet coalescence depends on an interaction time parameter which can be of great influence on the coalescence (or rupture) phenomenon. In order to be more efficient, the method should be coupled with subgrid modeling which can predict the interaction time parameter accurately. Note, moreover, that large computer resources are required for 3D studies.

Two main approaches are involved in the "front capturing" method, namely the Volume of Fluid method (VOF) and the level set method. The VOF method describes the volumetric fraction of each phase in grid cells. They were developed in the 1980s and have been commonly used for some years. The main difficulty of the method is that 2D interface reconstruction appears quite difficult, and 3D reconstruction is numerically prohibitive on 3D domain. A consequence can be some uncertainties on the interface curvature and thus on the surface tension forces. Nevertheless, let us mention that realistic and predictive simulations can be carried out (Rieber and Frohn, 1995; Gueyffier et al., 1999; Gueyffier, 2000). Interface reconstruction can be avoided by assuming a continuous volumetric fraction throughout the whole computational domain, which means that an interface thickness is introduced (Benkenida and Magnaudet, 2000). The method is then quite similar to the level set method in its continuous force formulation.

Osher and Sethian (1988) proposed a level set method which describes the interface with the zero level curve of a continuous function defined by the algebraic distance to the interface. To describe the interface discontinuities, two approaches can be used, namely the continuous force formulation ("delta" formulation), which assumes that the interface thickness is 2 or 3 grid meshes wide, and the ghost fluid method (GFM), which has been derived by Fedkiw et al. (1999) to capture jump condition on the interface. The two approaches are described here and the results are presented and discussed for the particular case of droplet collisions.

Experimental droplet collision studies (Ashgriz and Poo, 1990; Estrade, 1998) are providing us with different correlations to decide what happens when droplet collision occurs. The main parameters are the surface tension coefficient σ, liquid viscosity μ_l, liquid density ρ_l, droplet relative velocity U_c, the impact parameter I, and the ratio of droplet diameters Δ. The following non-dimensional numbers are thus defined by most authors to characterize droplet collisions, namely:

$$We = \frac{\rho_l U_c^2 D_s}{\sigma}, \quad Oh = \frac{\mu_l}{\sqrt{\rho_l \sigma D_s}}, \quad \Delta = \frac{D_s}{D_b}, \quad I = \frac{2b}{D_s + D_b} \tag{1}$$

where We is the Weber number and Oh the Ohnesorge number, and it is assumed that D_b is the bigger droplet diameter and D_s is smaller droplet diameter. The impact parameter I characterizes

the eccentricity of the collision, and b is defined as the distance from the center of one droplet to the relative velocity vector placed on the center of the other droplet. Note that the influence of gas density and gas viscosity (which are not involved in these parameters) on the collision regime has also been experimentally studied (Qian and Law, 1997).

Classification of collision regimes usually reports that five main types of collisions are observed as depicted in a (I, We) diagram (Fig. 1):

- coalescence after minor deformation (a),
- bouncing (b),
- coalescence after substantial deformation (c),
- coalescence followed by separation for near head-on collisions (d),
- coalescence followed by separation for off-center collisions (e).

Regime (a) occurs when the droplets' kinetic energy is small compared to surface energy, droplets are not deformed before colliding and coalescence is observed with few deformations.

Regime (b) is more difficult to handle: the droplets' energy is enough to induce surface deformations, but not enough to push out the gas film enclosed between droplet interfaces. The two interfaces remain separated by a very thin gas film which avoids coalescence and droplet bouncing occurs. This particular regime has been observed and explained in Jiang et al. (1992) for hydrocarbon droplets. However, it seems that it has never been observed for water droplets under ambient pressure and temperature conditions. Note that it has been experimentally proved that the physical properties of the gas play an important role in this collision regime: for example Qian and Law (1997) showed that bouncing can occur with water droplets for higher gas density than usually considered.

In regime (c) the droplets' kinetic energy is enough to push out the gas film trapped between droplet surfaces and coalescence is observed. The resulting droplet surface starts oscillating, but no secondary break up occurs.

When the droplets' kinetic energy is increased, regime (d) appears, droplet oscillations are greater, and break up is observed. In this regime, various behaviors can be obtained, and the number of

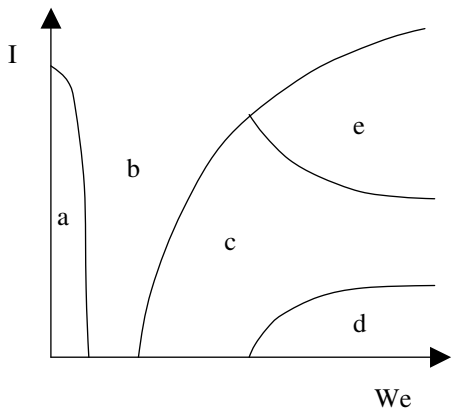

Fig. 1. (I, We) diagram for collision regime.

satellites in the break-up process increases with an increase of the Weber number (Ashgriz and Poo, 1990).

Finally, a fifth regime is observed for off-center collision. The three first regimes occur both for head-on collision and off-center collision, and regime (d), also called reflexive separation, occurs for a low impact parameter. Regime (e) occurs for energetic collision with a high impact parameter. Regime (e) differs from regime (d) on the break-up mechanism, which is linked to shear forces instead of oscillation forces.

The transition between these regimes can be characterized through a critical Weber number which depends on the impact parameter as it is observed in Fig. 1, but also on the properties of the gas and liquid phases. Viscosity, density and surface tension of the liquid phase are involved in the Ohnesorge number. Dependency of the critical Weber number with Ohnesorge number for transition between regime c (coalescence) and regime d (reflexive separation) will be illustrated in our results.

Experimental studies can help us in a better understanding of droplet collision mechanisms. However, due to the quite large number of parameters involved in the process, it remains of interest to develop predictive numerical methods to describe interface interactions. Moreover, the method described here is also well designed for spray atomization studies which are still a promising research goal for numerical simulations.

We first present the level set method and its coupling with incompressible Navier–Stokes equations. Both "delta" formulation and the ghost fluid method are described. Results are then presented and compared with experiments for different droplet collision configurations, namely regime (a), (c), (d), (e). Simulations are carried out with the 2D-axi code for head-on collisions and the 3D code for off-center collisions.

2. Numerical methods

2.1. Interface tracking

Level set methods are based on the transport of a continuous function ϕ which describes the interface between two mediums (Sussman et al., 1997; Sethian, 1999). That function is defined by the algebraic distance between any point of the domain and the interface. The interface is thus described by the 0 level of the level set function. Solving a convection equation determines the evolution of the interface in a given velocity field $\mathbf{V}$ (Sethian, 1999):

$$\frac{\partial \phi}{\partial t} + \mathbf{V} \cdot \nabla \phi = 0 \tag{2}$$

Particular attention must be paid to this transport equation. Some problems may arise when the level set method is developed: a high velocity gradient can produce wide spreading and stretching of the level sets, such that ϕ will no longer remains a distance function. A re-distancing algorithm (Sussman et al., 1997) is then applied to keep ϕ as the algebraic distance to the interface. The algorithm is based on the iterative resolution of the following equation:

$$\frac{\partial d}{\partial \tau} = \mathrm{sign}(\phi)(1 - |\nabla d|) = 0, \quad \text{where } \mathrm{d}(\mathbf{x}, t, \tau)_{\tau=0} = \phi(\mathbf{x}, t) \tag{3}$$

where τ is a fictitious time. We solve Eq. (3) until steady state is reached, thus close to the exact steady state solution namely either $\text{sign}(\phi) = 0$, meaning that we are on the droplet interface, or $|\nabla d| = 1$ which mathematically defines a distance function. We then replace $\phi(\mathbf{x}, t)$ by $\text{d}(\mathbf{x}, t, \tau_{\text{steady}})$. In our simulations two or three iterations per physical time step of re-distancing algorithm are sufficient to ensure that d is a signed distance. The main advantage of the above algorithm is to provide us with the required property for ϕ without changing its zero level set.

Eqs. (2) and (3) are hyperbolic types. Specific care must be devoted to the discretization method, as discontinuities are often observed in the results. To avoid singularities in the distance function field, we thus use a 5th order WENO scheme for convective terms (Jiang and Shu, 1996). Temporal derivatives are computed with at least a second order Runge–Kutta scheme.

One advantage of the level set method is its ability to represent topological changes both in 2D or 3D geometry quite naturally. Moreover, geometrical information on the interface, such as normal vector $\mathbf{n}$ or curvature κ, are easily obtained through:

$$\mathbf{n} = \frac{\nabla \phi}{|\nabla \phi|} \tag{4}$$

$$\kappa(\phi) = \nabla \cdot \mathbf{n} \tag{5}$$

It is well known that numerical computation of Eqs. (2) and (3) can generate mass loss in under-resolved regions. This is the main drawback of level set methods, but to improve mass conservation two main extensions of the method can be developed, namely the particle level set (Enright et al., 2002) and a coupling between VOF and level set (Sussman and Puckett, 2000). These extension have not been carried out here, but we have quantified mass loss in the simulations and ensured that it was negligible (<1%).

2.2. Projection method

The level set method is coupled with a projection method for the direct numerical simulation of incompressible Navier–Stokes equations expressed as follows:

$$\frac{\partial \mathbf{V}}{\partial t} + (\mathbf{V} \cdot \nabla)\mathbf{V} + \frac{\nabla p}{\rho(\phi)} = \frac{\nabla(2\mu(\phi)\mathbf{D})}{\rho(\phi)}, \quad \mathbf{D} = \frac{1}{2}(\nabla \mathbf{V} + \nabla \mathbf{V}^{\mathrm{T}}) \tag{6}$$

$$\nabla \cdot \mathbf{V} = 0 \tag{7}$$

p is the pressure, ρ and μ are the fluid density and viscosity respectively.

Three main steps are carried out in the projection method:

- estimate velocity $\mathbf{V}^*$ from velocity at time t_n (first order time discretization here assumed for simplicity):

$$\mathbf{V}^* = \mathbf{V}^n - \text{d}t\left((\mathbf{V}^n \cdot \nabla)\mathbf{V}^n - \frac{\nabla(2\mu(\phi^n)\mathbf{D})}{\rho(\phi^n)}\right) \tag{8}$$

- solve the Poisson equation for pressure:

$$\nabla \cdot \left(\frac{\nabla p^{n+1}}{\rho(\phi^{n+1})}\right) = \frac{\nabla \cdot \mathbf{V}^*}{\text{d}t} \tag{9}$$

• update divergence free velocities using pressure and intermediate velocity:

$$\mathbf{V}^{n+1} = \mathbf{V}^{*} - \mathrm{d}t\frac{\nabla p^{n+1}}{\rho(\phi^{n+1})} \tag{10}$$

In the projection method velocity components are expressed on a staggered grid. Spatial derivatives are estimated with a second order central scheme, but convective terms are also approximated by fifth order WENO scheme discretization in order to ensure a robust behavior of the solution. Temporal derivatives are approximated with at least a second order Runge–Kutta scheme or Adams Bashforth algorithm.

Poisson equation discretization, with a second order central scheme, leads to a linear system; the system matrix is symmetric and positive definite with five diagonals. Different methods can be derived to solve that system. According to different authors (Tatebe, 1996), the multigrid method for preconditioning conjugate gradient methods (MGCG) combines incomplete choleski conjugate gradient (ICCG) robustness with the multigrid fast convergence rate. We have thus developed the MGCG method in our code and greatly decreased computational time compared to the ICCG algorithm.

2.3. Discontinuities

The interface is defined by two different phases and discontinuities must be taken into account for density, viscosity and pressure. Specific treatment is thus needed to describe the jump conditions numerically. Formally, these conditions are defined by:

$$\lambda(\phi) = \lambda_{\mathrm{g}} + (\lambda_{\mathrm{l}} - \lambda_{\mathrm{g}})H(\phi) \tag{11}$$

where λ stands for ρ or μ and $H(\phi)$ is the Heaviside function centered on the interface.

The pressure jump related to surface tension σ and to the interface curvature reads (Tanguy, 2004):

$$[p] = \sigma\kappa(\phi) + 2[\mu]\ (\nabla u \cdot \mathbf{n}, \nabla v \cdot \mathbf{n}, \nabla w \cdot \mathbf{n}) \cdot \mathbf{n} \tag{12}$$

where $[\cdot]$ represents a jump in the variable considered.

Two different approaches can be used to represent the above conditions, namely the continuum surface force (delta formulation) or the ghost fluid method.

2.3.1. Continuum surface force

In the continuum surface force (CSF) approach, the Heaviside function is smoothed on two or three nodes on each side of the interface, as follows:

$$H_{\varepsilon}(\phi) = \begin{cases} 0 & \text{if } \phi < \varepsilon \\ \dfrac{1}{2}\left[1 + \dfrac{\phi}{\varepsilon} + \dfrac{1}{\pi}\sin\left(\dfrac{\pi\phi}{\varepsilon}\right)\right] & \text{if } |\phi| \leqslant \varepsilon \\ 1 & \text{if } \phi > \varepsilon \end{cases} \tag{13}$$

where $\varepsilon = 1.5\,\mathrm{d}x$.

In order to take into account surface tension force, an additional term is involved in Navier–Stokes equations (Eq. (8)), which is written (Smereka, 1996):

$$-\sigma\kappa(\phi)\delta_\varepsilon(\phi)\nabla\phi \tag{14}$$

where δ_ε is the derivative of $H_\varepsilon(\phi)$.

That approach has been proved to be robust and leads to interesting results. But smoothing the Heaviside function introduces an interface thickness which depends on the mesh size, and thus an uncertainty on the exact location of the interface.

2.3.2. Ghost fluid method

To overcome that smoothing, the ghost fluid method (GFM), has been developed by Fedkiw et al. (1999). The formalism respects jump discontinuities across the interface, and avoids an interface thickness. Discretization of discontinuous variables is more accurate, and spurious currents in the velocity field are thus much lower than with CSF methods. We have used this procedure to discretize all discontinuous variables, namely density, viscosity, pressure and viscous tensors (Kang et al., 2000; Tanguy, 2004).

In the GFM methods, ghost cells are defined on each side of the interface (Liu et al., 2000; Kang et al., 2000) and appropriate schemes are applied for jump conditions. As defined above, the interface is characterized through the distance function, and jump conditions are extrapolated on some nodes on each side of the interface. Following the jump conditions, the discontinued functions are extended continuously and then derivatives are estimated.

In order to explain the process in a very simple case, let us consider variable f which is discontinuous across the interface in the Ω domain such that the jump of f is $[f]_\Gamma = a_\Gamma$ (Fig. 2).

To solve the simple equation $\mathrm{d}^2f/\mathrm{d}x^2 = 0$, specific discretization is applied depending on the interface location. When the interface is localized between x_i and x_{i+1}, f derivatives at i and $i+1$ nodes are expressed by:

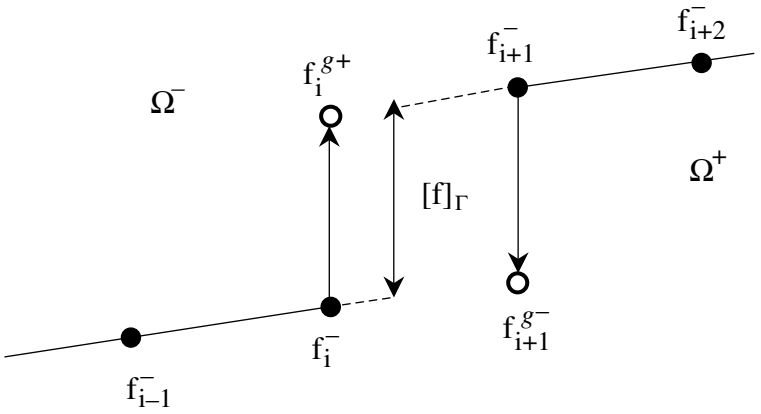

Fig. 2. Ghost values due to jump in variable f.

$$\frac{\frac{(f^+_{i+1}-f^-_i)}{\mathrm{d}x}-\frac{(f^-_i-f^-_{i-1})}{\mathrm{d}x}}{\mathrm{d}x}=0 \tag{15}$$

$$\frac{\frac{(f^+_{i+2}-f^+_{i+1})}{\mathrm{d}x}-\frac{(f^+_{i+1}-f^-_i)}{\mathrm{d}x}}{\mathrm{d}x}=0 \tag{16}$$

Due to the jump of f between i and $i+1$, ghost values for f^+_{i+1} in Eq. (15) (f^{g-}_{i+1}) and f^-_i in Eq. (16) (f^{g+}_i) are defined by:

$$\begin{aligned} f^{g-}_{i+1} &= f^+_{i+1}-a_\Gamma \\ f^{g+}_i &= f^-_i+a_\Gamma \end{aligned} \tag{17}$$

The finite difference form of $\mathrm{d}^2f/\mathrm{d}x^2=0$ is thus:

$$\frac{(f_{i+1}-2f_i+f_{i-1})}{\mathrm{d}x^2}=0 \quad \text{when no jump occurs between } i \text{ and } i+1 \tag{18}$$

In cells that are crossed by the interface equation reads:

$$\frac{(f_{i+1}-2f_i+f_{i-1})}{\mathrm{d}x^2}=\frac{a_\Gamma}{\mathrm{d}x^2} \tag{19}$$

The above scheme can be applied for any kind of discontinuities, assuming that the interface can be localized inside a grid mesh and that the jump of the discontinuous variables is known. More details can be found in Liu et al. (2000) on implementing the ghost fluid method to solve the Poisson equation with discontinuous coefficients and obtain solution with jump condition. The method has been used to compute two-phase flows, and it compares favorably with the Continuum Surface Method in both 2D and 3D cases. It is clearly shown that spurious currents are 10^3 times lower with GFM than with CSF for a static drop (Tanguy, 2004). Moreover in our simulations we find that very thin interfacial structures are better resolved when using the ghost fluid method. All the simulations presented here are thus carried out with the ghost fluid method. Numerical codes have been developed for 2D, 2D-axi and 3D geometries, and MPI parallelization is used.

3. Results for head-on droplet collision

As previously mentioned, mass conservation might not be satisfied in level set methods and we thus evaluated mass loss during all simulations to check that it was negligible (<1%). Moreover we carried out convergence tests to check that coalescence and break-up of interface was independent of the mesh size. Initially, droplet velocity was imposed to fit the given Weber number. The gas phase is air and the liquid phase is ethanol or water. The physical properties of both phases are given in Table 1.

3.1. Coalescence after minor deformation

The ethanol droplet diameter is 200 μm and the initial relative velocity is 0.4 $\mathrm{m\,s^{-1}}$. The Weber number is thus equal to 2.2 and the Ohnesorge number is 0.014. The grid is 500 μm × 1500 μm

Table 1
Physical properties of both phases

	σ (kg s^{-2})	ρ (kg m^{-3})	μ (kg m^{-1} s^{-1})
Air	–	1.226	1.78×10^{-5}
Water	0.072	1000	0.001137
Ethanol	0.02275	791	0.0012

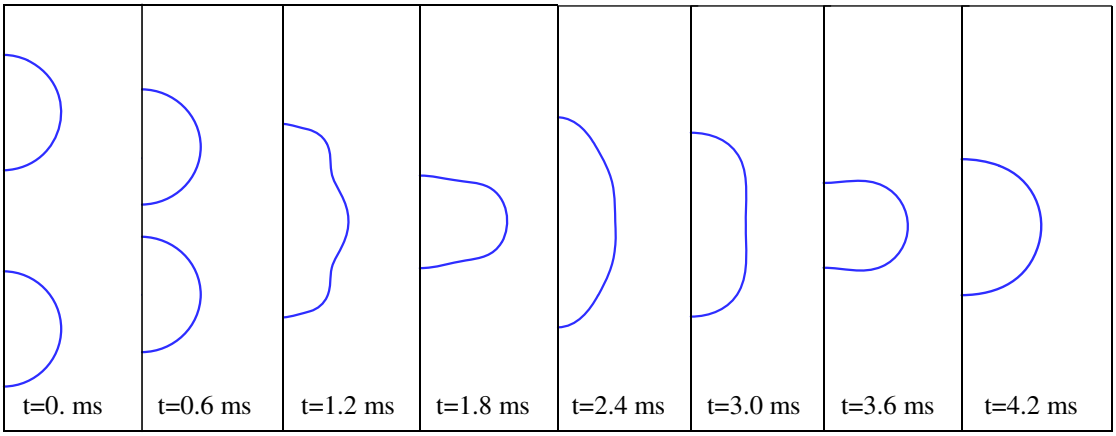

Fig. 3. 200 μm ethanol droplet collision for $We = 2.2$, $Oh = 0.014$.

square and two different grid sizes are used, namely 40×120 and 80×240 in order to ensure that the grid is independent of topological changes. The time step is determined from CFL conditions as proposed by Fedkiw et al. (1999).

Fig. 3 presents the temporal evolution of the interface for the 80×240 grid and the time step between two drawings is 0.6 ms. We observe the coalescence of the two droplets and the resulting drop then starts to oscillate slightly but the momentum energy is too low to produce any break-up in the process. Two interface profiles are drawn in Fig. 4 for the two different mesh sizes. We clearly observe that the results are almost identical and space convergence is reached. Moreover mass loss has been evaluated and is less than 0.09% on the 80×240 grid.

3.2. Coalescence after substantial deformation

The above conditions are kept, but the relative velocity is set to 1.1 m s^{-1} and the Weber number is equal to 16.8. Grid sizes are 60×180 and 90×270 nodes respectively.

When compared to the previous case, a quite similar behavior is observed (Fig. 5), but the oscillations of the resulting droplet are much greater. As expected, the drop behavior is driven by surface tension forces. Due to the high curvature at impact, the drop is elongated in the perpendicular direction of collision and when it reaches its maximum elongation, the surface tension tends to draw back the droplet to its more stable shape and oscillations thus occur around the spherical shape. However, the initial kinetic energy of the droplets is still not enough to induce break up of the cylinder shape observed on the fifth drawing.

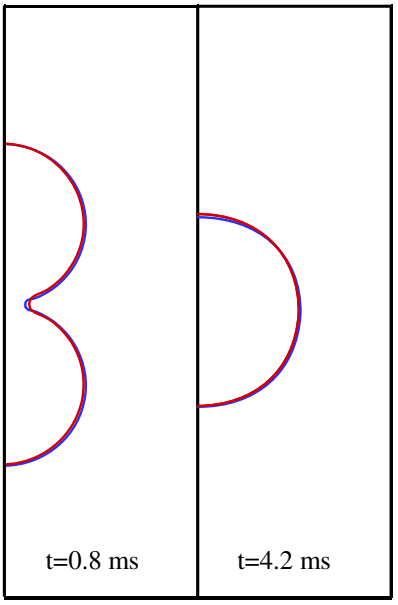

Fig. 4. Interface profiles for 40×120 (red) and 80×240 (blue) grids. (For interpretation of the references in colour in this figure legend, the reader is referred to the web version of this article.)

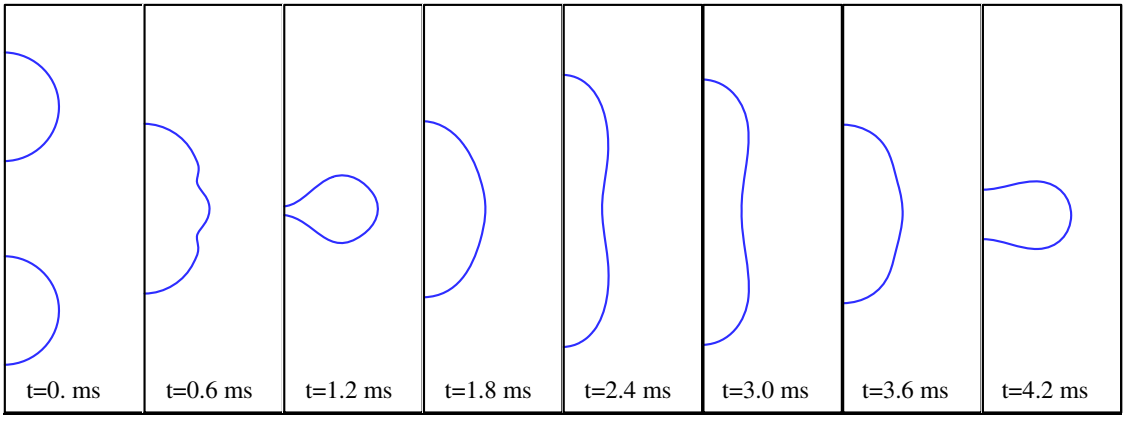

Fig. 5. 200 μm ethanol droplet collision for $We = 16.8$, $Oh = 0.014$.

Three interface profiles are presented in Fig. 6 for the two grid meshes. A very slight difference is observed on the first profile for the thin membrane, but without any influence on the coalescence process observed on the next profiles. Mass loss on the 90×270 grid is less than 0.13%. Note that symmetry of the collision process is kept all along the collision and it will now be introduced as the bottom axis boundary condition for head-on collisions of identical droplets.

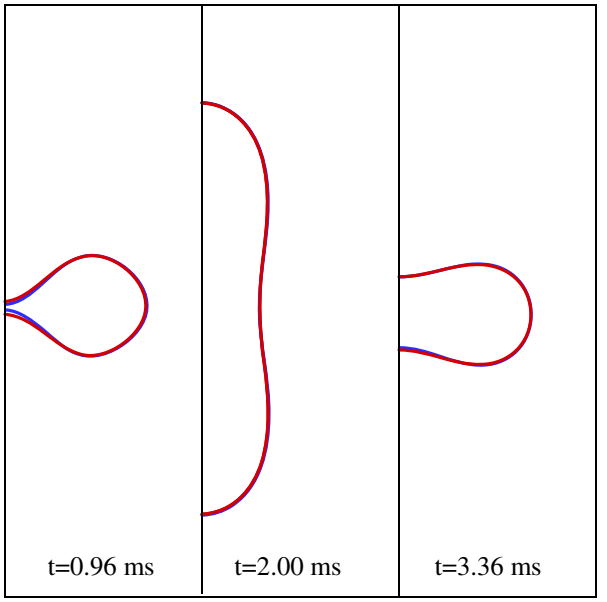

Fig. 6. Interface profiles for 60×180 (red) and 90×270 (blue) grids. (For interpretation of the references in colour in this figure legend, the reader is referred to the web version of this article.)

3.3. Coalescence followed by separation for head-on collisions

We increase the Weber number up to 61, through an increase of the relative velocity which is equal to $2.1\,\mathrm{m\,s^{-1}}$. The grid size is $500\,\mu\mathrm{m} \times 1500\,\mu\mathrm{m}$ and grid resolution is 90×270 and 180×540.

Fig. 7 shows the interface behavior with a 0.25 ms time step between each plot. We recall that the symmetry condition is now applied on the axis.

We first observe the coalescence of the two droplets (image 2) and the resulting single drop then stretches into a ring shape with a thin membrane (image 4). Under surface tension forces, the ring is then attracted to its center (image 5) and the internal motion of the liquid leads to a cylinder (image 8). Due to the fairly high initial kinetic energy of the droplets, the cylinder is then lengthens (image 11) until break-up occurs (image 12). A satellite appears and the three resulting droplets then slightly oscillate before recovering a spherical shape.

In Fig. 8 we plot the interface profiles just before and after the break-up for the two grid sizes. The figure clearly shows that the grid resolution here is sufficient, as the topological change is almost the same for the two grid meshes. Mass loss on the 90×270 grid is less than 0.71%.

4. Comparisons with experiments

The results presented in the previous section are in good agreement with experimental observations from Ashgriz and Poo (1990) on water droplets and Estrade (1998) on ethanol droplets. They state that the coalescence regime is obtained for $We < 19$ (Ashgriz and Poo) or $We < 31$

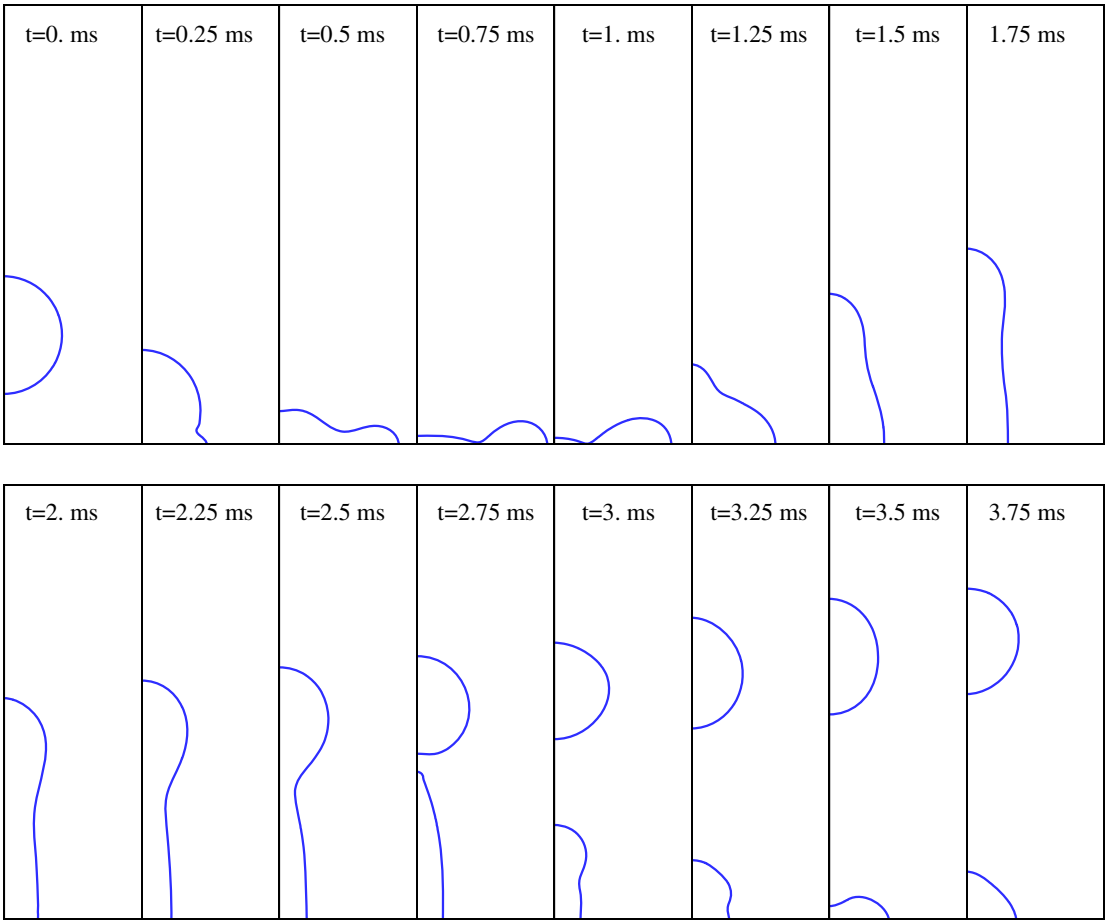

Fig. 7. 200 μm ethanol droplet collision for $We = 61$, $Oh = 0.014$.

(Estrade). They also observed that for $We = 61$ the collision process leads to the break-up of the resulting droplet with the formation of one satellite. The aim of the present section is to compare our simulations with experimental results, but a quantitative comparison remains quite difficult due to the many problems encountered in experimental studies. One reason is the lack of precise experimental conditions, where the Weber number is known but where we have no reliable information on droplet diameters or velocities (the Reynolds and Ohnesorge numbers are unknown). In our simulation we thus try to be as close as possible to experiments by taking the given Weber number and guessing the droplet diameter from the injector nozzle size. Another problem comes from some uncertainties on measurements, such as the impact parameter (for example close to 0, but not a perfect head-on collision) or physical properties of the liquid, namely the surface tension which is very sensitive to the purity of the water. Moreover, no time scale on the image sequences is available. However qualitative comparisons can be carried out, mainly with Ashgriz and Poo's (1990) results, as they provide good quality pictures for the different collision processes. We thus present comparisons of droplet shapes in the collision process between our simulation and Ashgriz and Poo (1990) results.

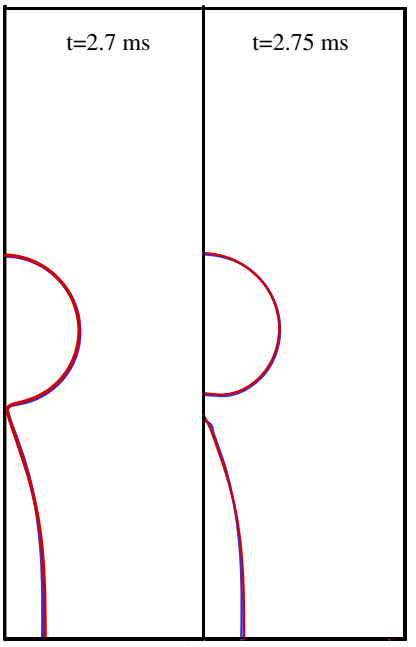

Fig. 8. Interface profiles for 90×270 (red) and 180×540 (blue) grid. (For interpretation of the references in colour in this figure legend, the reader is referred to the web version of this article.)

4.1. Coalescence followed by separation for head-on collisions

Collision has been observed by Ashgriz and Poo for two identical water droplets, with a Weber number equal to 23, and impact parameter nearly equal to zero (0.05). Simulation results are presented for water droplets, with the same Weber number, and with an impact parameter equal to 0, a droplet radius of 400 μm, and a droplet relative velocity of 1.44 $\mathrm{m\,s^{-1}}$. The grid size is 60×120 in the 2D-axi configuration.

Comparisons between our results and experimental visualization are shown in Fig. 9a and b.

The qualitative agreement between simulation and experiments in the different pictures is quite good. The final state is well predicted (two droplets without satellites) and moreover, the liquid phase behavior during the collision process is very similar in both image sequences.

4.2. Coalescence followed by separation with formation of one satellite for head-on collisions

In the same conditions, Ashgriz and Poo first increased the Weber number up to 40. We thus kept the same simulation conditions, and only changed the droplet's relative velocity to 1.9 $\mathrm{m\,s^{-1}}$ to fit the Weber number. The grid size is also the same, 80×160.

We can also observe in Fig. 10a and b the good qualitative agreement in the image sequences. However, it appears that the satellite is slightly smaller in the simulation than in the experiments but, as previously mentioned, precise experimental data are required to discuss the results further.

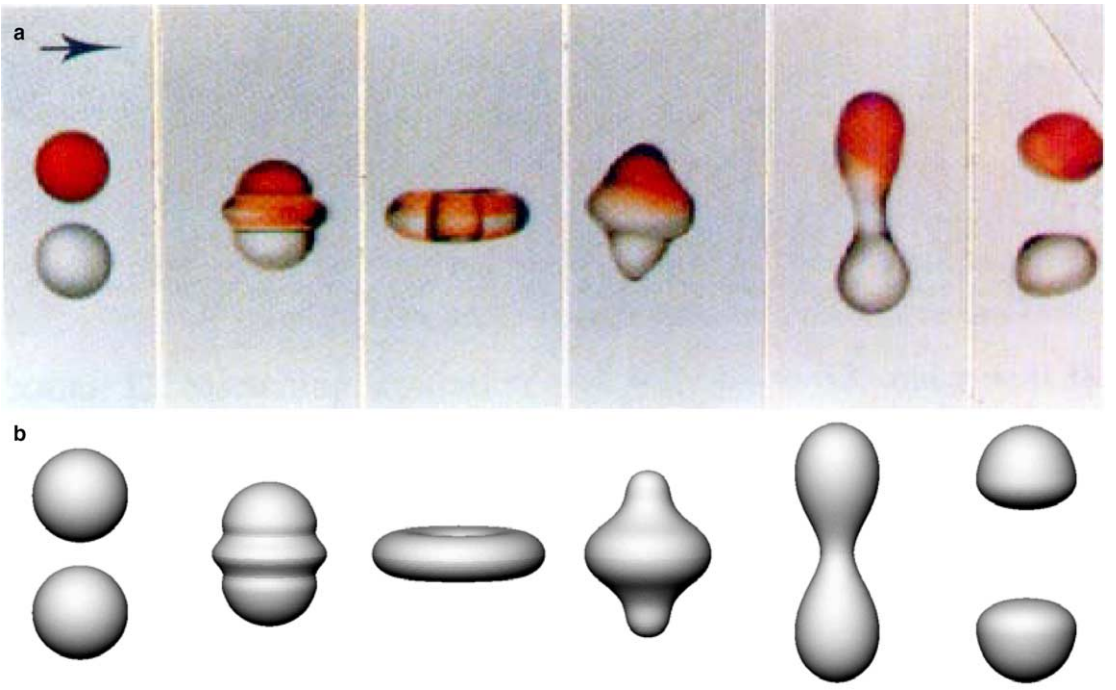

Fig. 9. (a) Head-on collision, $We = 23$, from Ashgriz and Poo (1990). (b) Head-on collision, $We = 23$, $Oh = 0.0047$, our simulation.

4.3. Head-on collision for two droplets with different sizes

In order to confirm the ability of our code to describe droplet collisions, the third case concerns the head-on collision of two droplets of unequal diameters. The experimental conditions given by Ashgriz and Poo are the Weber number ($We = 56$), the droplet radius ratio (0.5) and the impact parameter (0). We fixed the largest radius at 400 μm, and the smallest radius at 200 μm; the relative velocity for $We = 56$ is thus equal to 3.175 $\mathrm{m\,s^{-1}}$. The grid size is 60×240.

As can be observed in Fig. 11a and b the agreement between the experimental pictures and the simulation results is very impressive. The shape evolution of the liquid phase is quite identical on both image sequences, and the last images of the two resulting droplets prove the quality of the whole collision process simulation.

4.4. Off-center collision

In order to check the method in 3D configurations, collision between two droplets with a non-zero impact parameter has been studied. We chose ethanol droplets, with a radius of 100 μm, impact parameter of 0.5 and relative velocity of 2.94 $\mathrm{m\,s^{-1}}$; this gives a Weber number equal to 60. The grid size is $64 \times 128 \times 256$ and the symmetry condition is imposed on the parallel direction of the droplet velocity vectors. MPI parallelization is used and calculations are carried out on eight processors on an IBM 1600 cluster.

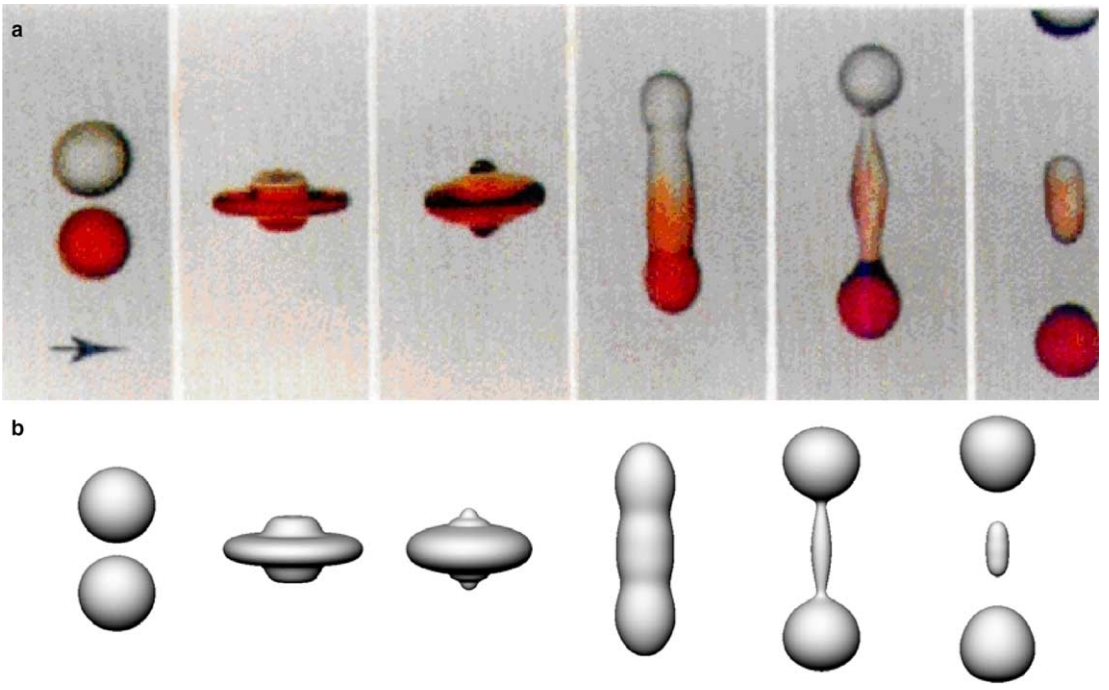

Fig. 10. (a) Head-on collision, $We = 40$, from Ashgriz and Poo (1990). (b) Head-on collision, $We = 40$, $Oh = 0.0047$, our simulation.

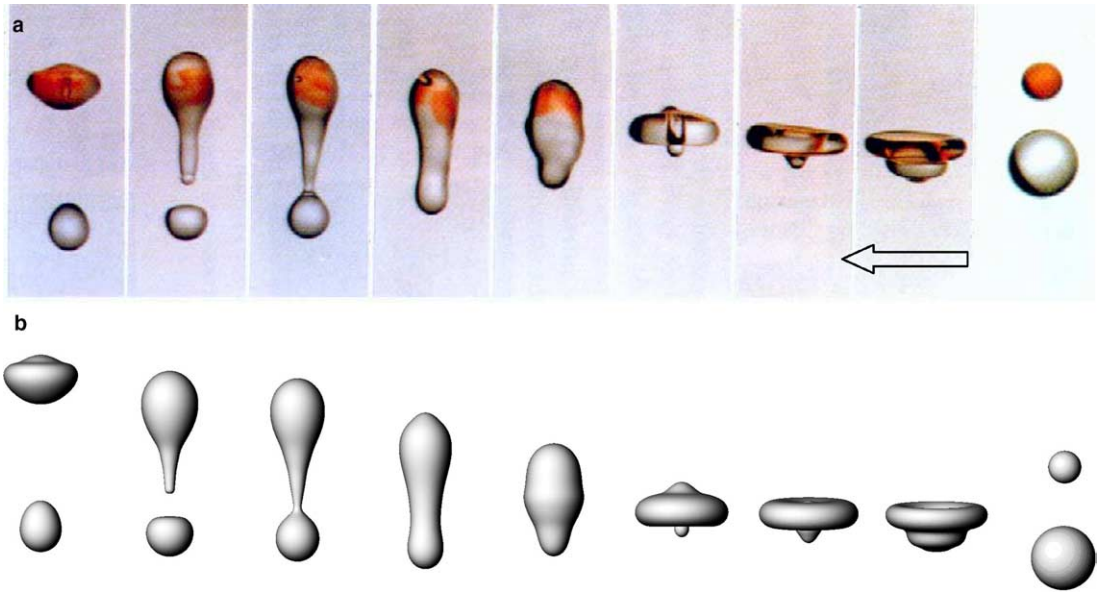

Fig. 11. (a) Head-on collision, $We = 56$, radius ratio 0.5 from Ashgriz and Poo. (b) Head-on collision, $We = 56$, $Oh = 0.0047$, radius ratio 0.5, our simulation.

Simulation results are presented in Fig. 12a. The collision process leads to coalescence followed by separation with the formation of two satellites. The chosen initial configuration is in the transition regime between separation with the formation of one satellite and separation with the formation of three satellites, as observed by Estrade (1998).

Going back to Ashgriz and Poo, the authors showed a collision with very similar behavior as shown in Fig. 12b, but with a slightly different configuration, namely water droplets, $We = 83$ and impact parameter is 0.43. A difference appears on image 2 in Fig. 12a and b where the thin membrane is broken in the simulation but seems to experimentally remain during the collision.

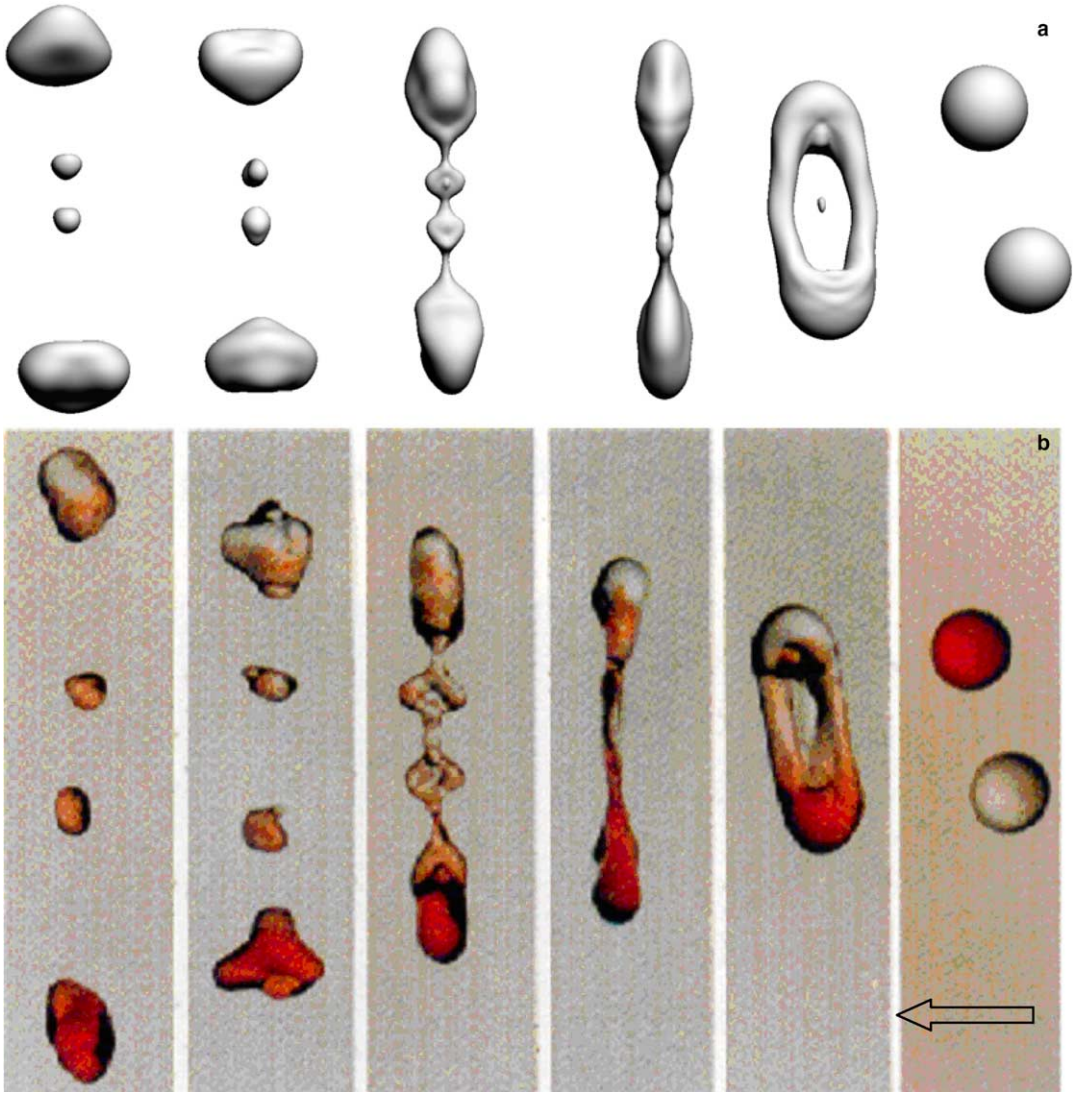

Fig. 12. (a) 3D simulation, ethanol droplet, $We = 60$, $Oh = 0.02$, impact parameter 0.5. (b) Water droplet, $We = 83$, impact parameter 0.43 from Ashgriz and Poo (1990).

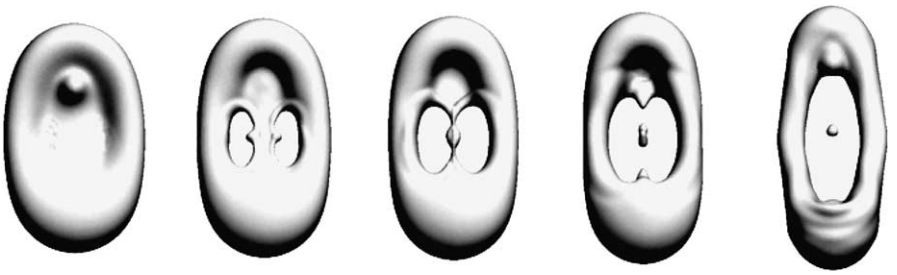

Fig. 13. Thin membrane break in 3D simulation.

The numerical description of very thin liquid layers in the collision process is a difficult problem to handle. As shown in Fig. 13 the thin membrane which is observed in the 3D simulation first breaks near the liquid ring, and then the bridge on the center of the liquid shape is elongated until it also breaks and a small droplet appears in the center. The ring is then stretched until its two sides collapse on the vertical axis and the small droplet is captured and merges with the whole liquid.

Ashgriz and Poo never seem to observe this behavior. We can assume that the break-up in the interface topology is induced by under-resolved numerical simulation of the very thin interface. However, while it remains quite impossible to check the spatial convergence of the results in 3D configurations, such behavior has also been observed in 2D simulations, namely for $We = 23$ in the above results. Refining the grid can, in some cases, allow the interface motion to be described without any rupture, but we found some cases where the membrane break-up occurs at the same time on the same location whatever the grid size we used (the finest grid mesh was less than 2 μm). We observed that these thin membranes rupture during head-on droplet collisions for quite small Weber numbers. Fig. 14 can help to propose an explanation for this behavior in the simulations.

For a small Weber number ($We = 23$, blue curve[1]) the kinetic energy of the liquid phase is not sufficient to push a large amount of liquid away with the ring, and generates a tore with a very thin inside membrane. Then the ring tends to recover its natural form under surface tension forces, namely a cylindrical tore and this induces the rupture of the membrane on the inside edge of the ring before it contracts.

For a higher Weber number ($We = 125$, red curve), the resulting liquid sheet is wider and thinner and the liquid then goes back towards the center of the ring without any rupture of the membrane.

Note that the surface energy of the inside membrane is negligible due to its curvature which tends towards 0. Moreover, the rupture of the very thin membrane does not induce much difference in the qualitative characteristics of the collision. There is still a possibility that this rupture might disappear if by the grid is refined; and automatic mesh refinement (AMR) would be of interest to help in deciding whether the membrane ruptures or not.

[1] For interpretation of colour in Fig. 14, the reader is referred to the web version of this article.

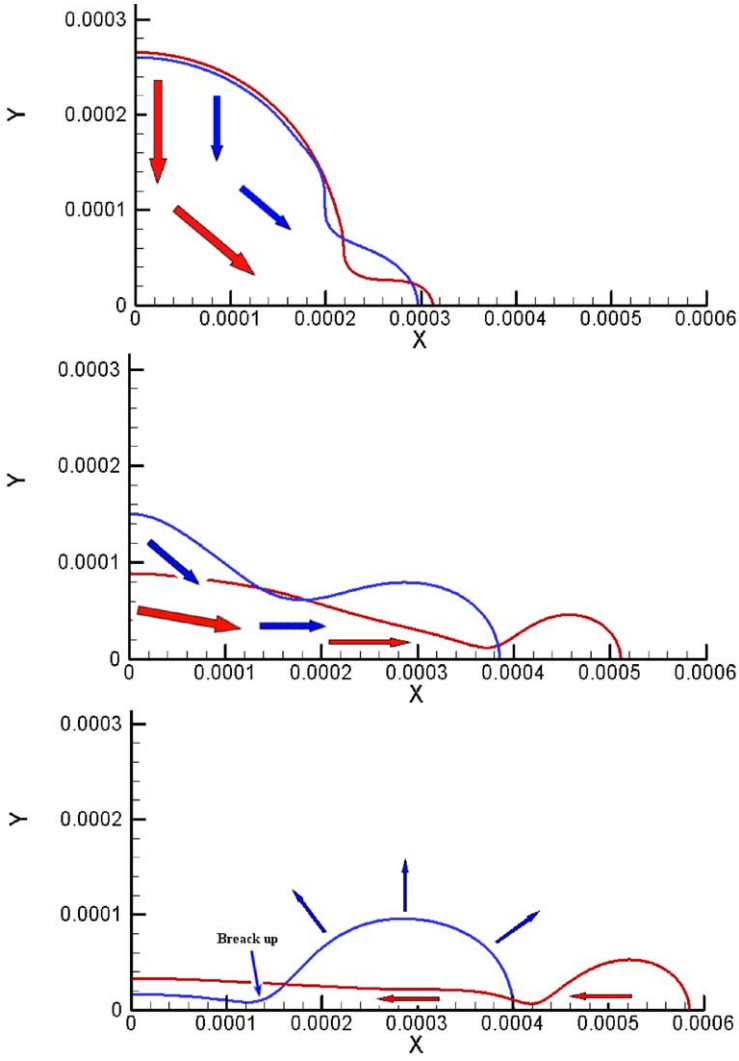

Fig. 14. Thin layer during head-on droplet collision.

4.5. Quantitative comparison

As previously mentioned, quantitative comparisons can be biased by a lack of experimental operating conditions or detailed measurement data. However experimental studies (Estrade, 1998; Qian and Law, 1997) provide the critical Weber versus Ohnesorge number for the transition between coalescence regime and separation regime for droplet head-on collision (regimes (c) and (d) in Fig. 1). Fig. 15 compares our results with Qian and Law (1997) and Estrade (1998) experimental correlations, and Rieber and Frohn (1995) simulations. The agreement between our simulations and experimental data is very satisfactory and confirms that level set method with ghost fluid approach are accurate tools numerical simulations of droplet collisions.

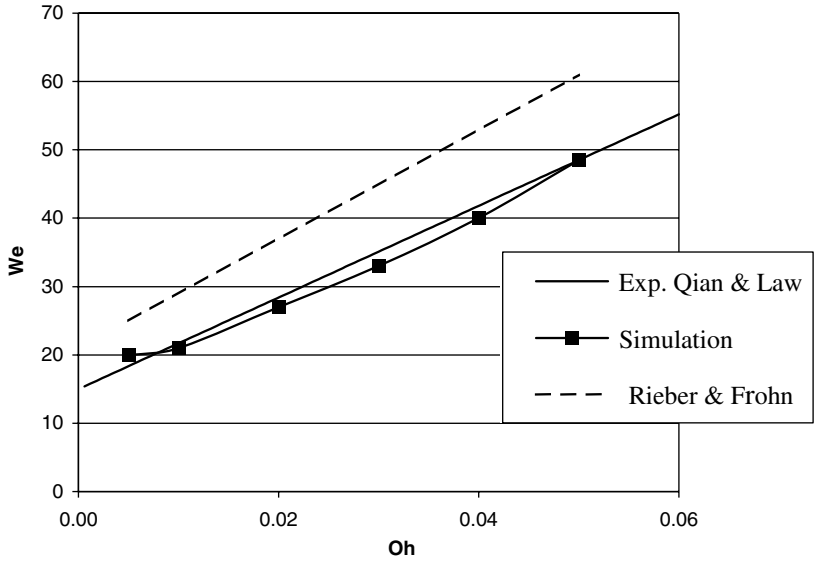

Fig. 15. Comparison between numerical and experimental results for the transition between coalescence and separation in (Oh, We) space for droplet head-on collision.

5. Conclusion

Level set methods are based on defining a continuous function such that its zero level curve is the interface. That function is initialized as the signed distance to the interface in the computation field. Solving a convection equation allows the interface displacements in a given velocity field to be followed. One advantage of the level set method is its ability to represent topological changes, both in 2D or 3D geometry, quite naturally. Moreover, the geometrical properties of the interface, such as the normal vector or curvature, are easily obtained through the level set function gradient. To avoid spreading and stretching of the level set, a re-distancing algorithm is applied to ensure that the function remains the algebraic distance to the interface.

The level set method is coupled with a projection method for the direct numerical simulation of the incompressible Navier–Stokes. Spatial derivatives are estimated with a second order central scheme, but convective terms are approximated by fifsth order WENO scheme discretization in order to obtain robust behavior of the solution. Temporal derivatives are approximated with at least a second order Runge–Kutta scheme or an Adams Bashforth formulation. The linear system deduced from the Poisson equation is solved with a multigrid algorithm for preconditioning the conjugate gradient method.

Two different approaches can be used to handle interface discontinuities, namely the ghost fluid method and the continuum surface force (delta formulation). In delta formulation an interface smoothing is induced on two or three grid nodes, and the ghost fluid method takes into account the discontinuities through variable continuous extension on both side of the interface. The ghost fluid method is preferred here for drop collision simulations. All the comparisons with experimental studies are in very good agreement and some of them are very impressive. However, further developments are required. The main drawback of the method is possible mass loss for the

under-resolved zone of the computational domain. We have checked in the results presented that mass conservation is better than 1% by refining the grid. It clearly appears that grid size limitations do not allow the same strategy for 3D simulations. A promising development is the coupling of the ghost fluid and VOF/level set methods (Sussman and Puckett, 2000), in order to benefit from both the precise interface characterization of the GFM and from the mass conservation of VOF.

Acknowledgments

Simulations were carried out at the CRIHAN (Centre de Ressources Informatiques de Haute Normandie) and the IDRIS (Institut du Développement et des Ressources en Informatique Scientifique). We thank also Ms. D. Moscato for improving English writing.

References

Ashgriz, N., Poo, J.Y., 1990. Coalescence and separation in binary collisions of liquid drops. J. Fluid Mech. 221, 183–204.

Benkenida, A., Magnaudet, J., 2000. A method for the simulation of two-phase flows without interface reconstruction. Comptes Rendus de l'Academie des Sciences Series IIB Mechanics Physics Astronomy, vol. 328, 25–32.

Enright, D., Fedkiw, R., Ferziger, J., Mitchell, I., 2002. A hybrid particle level set method for improved interface capturing. J. Comput. Phys. 183, 83–116.

Estrade, J.P., 1998. Etude expérimentale et numérique de la collision de gouttelettes. PhD thesis, ONERA Toulouse.

Fedkiw, R., Aslam, T., Merriman, B., Osher, S., 1999. A non-oscillatory eulerian approach to interfaces in multimaterial flows (the ghost fluid method). J. Comput. Phys. 152, 457–492.

Gueyffier, D., 2000. Etude de l'impact de gouttes sur un film liquide mince. PhD thesis, Université Paris 6, Laboratoire de Modélisation en Mécanique.

Gueyffier, D., Li, J., Nadim, A., Scardovelli, S., Zaleski, S., 1999. Volume of fluid interface tracking with smoothed surface stress methods for three-dimensional flows. J. Comput. Phys. 152, 423–456.

Jiang, G.S., Shu, C.W., 1996. Efficient implementation of weighted essentially non-oscillatory schemes. J. Comput. Phys. 126, 202–228.

Jiang, Y.J., Umemura, A., Law, C.K., 1992. An experimental investigation on the collision behaviour of hydrocarbon droplets. J. Fluid Mech. 234, 171–190.

Kang, M., Fedkiw, R., Liu, X.D., 2000. A boundary condition capturing method for multiphase incompressible flow. J. Sci. Comput. 15, 323–360.

Liu, X.D., Fedkiw, R., Kang, M., 2000. A boundary condition capturing method for Poisson equation on irregular domains. J. Sci. Phys., 151–178.

Nobari, M.R., Jan, Y.J., Tryggvason, G., 1996. Head-on collision of drops—a numerical investigation. Phys. Fluids 8, 1.

Osher, S., Sethian, J.A., 1988. Fronts propagating with curvature-dependent speed: algorithms based on Hamilton–Jacobi formulations. J. Comput. Phys. 79, 12–49.

Qian, J., Law, C.K., 1997. Regimes of coalescence and separation in droplet collision. J. Fluid Mech. 331, 59–80.

Rieber, M., Frohn, A., 1995. Navier–Stokes simulation of droplet collision dynamics. Aerosol Sci. 26, S929–S930.

Sethian, J.A., 1999. Level Set Method and Fast Marching Methods. Cambridge University Press.

Smereka, P., 1996. Level set methods for two-fluid flows. Lecture notes from course Méthodes Numériques pour les Écoulements Diphasiques, 18–21 Novembre 1996, INRIA—Rocquencourt France.

Sussman, M., Puckett, E.G., 2000. A coupled level set and volume-of-fluid method for computing 3D and axisymmetric incompressible two-phase flows. J. Comput. Phys. 162, 301–337.

Sussman, M., Fatemi, E., Smereka, P., Osher, S., 1997. An improved level set method for incompressible two-phase. Comput. Fluids 27.

Tanguy, S., 2004. Développement d'une méthode de suivi d'interface. Applications aux écoulements diphasiques. PhD thesis, Université Rouen, Laboratoire CORIA CNRS UMR 6614.

Tatebe, O., 1996. The Multigrid Preconditioned Conjugate Gradient Method. PhD thesis, University of Tokyo.